Structure of an Evolving Hailstorm, Part I: General Characteristics and Cellular Structure

J.-P. CHALON,[1] J. C. FANKHAUSER AND P. J. ECCLES

National Center for Atmospheric Research,[2] Boulder, Colo. 80303

(Manuscript received 17 September 1975, in revised form 16 December 1975)

ABSTRACT

The detailed structure and evolution of radar echoes observed in a multicellular hailstorm are analyzed. General environmental conditions, overall radar echo development, and precipitation measurements are briefly discussed, but the analysis is mainly concerned with a particular event which was thoroughly observed by several different field facilities of the National Hail Research Experiment. This hailstorm, which evolved in a systematic and periodic manner, is the subject of four companion papers appearing in this issue.

Overall storm characteristics are found to compare closely to earlier descriptions of multicell hailstorms occurring in the High Plains. The motion of the main system was to the right of the mean wind vector in the cloud layer. Cell velocity was along but less than the wind in the mid-troposphere. Propagation by new cell growth in a preferred location with respect to existing radar echoes dominated the motion of the overall system. Study of the formation and evolution of individual cells showed that discrete new echoes formed near the altitude of 7 km MSL (−12°C) on the storm's right forward flank 5 to 10 km ahead of existing echo components at approximately 15 min intervals. Each grew rapidly in intensity and height and by moving more slowly than the overall echo complex soon became the main storm component. Average lifetime of individual cells, including the period from visually perceptible turrets, to "first echo," to echo decay, was 45 min. Thus, as many as three cells were found to coexist in varying stages of development. The ascent rate of visual cloud turrets and the history of maximum radar reflectivity of individual cells after the appearance of first echo indicate that the longest in-cloud residence time available for particle growth to the largest observed hail size (1.5 cm diameter) was between 30 and 35 min.

1. Introduction

One of the objectives of the National Hail Research Experiment (NHRE) is the definition of thermodynamic structure and airflow patterns characteristic of the different types of hail-producing thunderstorms. Aside from the motivation of gaining increased understanding of all aspects of convective cloud dynamics, incisive case studies are required to establish a firmer physical basis for conduct and evaluation of a hail suppression experiment. Of particular importance is the interdependence between airflow patterns and the manner in which precipitation products are generated, dispersed, and deposited at the ground. To establish the interrelationship of the important hailstorm parameters it is necessary to adopt a case study approach wherein many observational techniques are brought to bear simultaneously on the same storm. Because of the sophistication of the required observational techniques, the difficulties in coordinating them, and the infrequency of large hailstorms within the compass of fixed instrumentation, an adequately comprehensive data base is only occasionally achieved.

On 9 July 1973 a number of thunderstorms moved over and produced hail within the field facilities of NHRE located in northeastern Colorado. A full complement of observing systems, including conventional and Doppler radars, surface and upper-air networks, and instrumented aircraft, gathered data pertinent to a particular unseeded multicell storm near the town of Raymer. This paper is the first of a series of five appearing in this issue which describes the diverse observations (Parts I, II, III, and IV) and which culminates in a synthesis of the airflow and associated microphysical processes relevant to hail formation in multicell storms (Part V).

We present a brief review of significant larger scale features, the general radar echo development patterns as they occurred on this day, and some characteristics of the precipitation, but our analysis here concerns mainly the detailed radar echo structure and evolution in the multicell storm which was the focus of the other observations. Our primary data base is the three-dimensional radar reflectivity patterns produced by

[1] Scientific visitor on leave from Météorologie Nationale, Paris, France, on a fellowship from the Délégation Générale à la Recherche Scientifique et Technique.

[2] This research was performed as part of the National Hail Research Experiment, managed by the National Center for Atmospheric Research and sponsored by the Weather Modification Program, Research Applications Directorate, National Science Foundation.

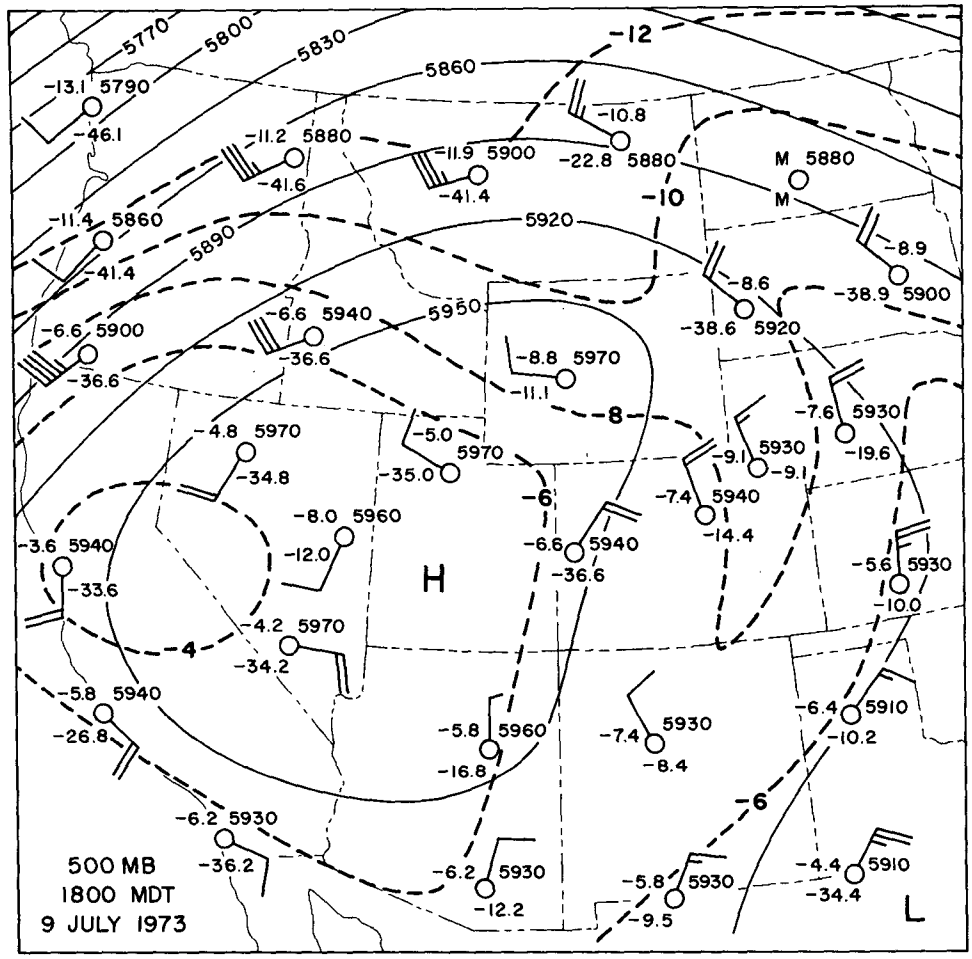

FIG. 1. 500 mb height contours (m), and isotherms (°C); 1800 MDT, 9 July (0000 GMT, 10 July) 1973. At stations, plotted data include temperature, dew point, height, and winds (a full barb is 10 m s^{-1}).

computer using digital data from high-speed raster scans by the NHRE S-band research radar located near Grover, Colo. A complete set of PPI scans was available from near ground level to storm top at an average interval of 2 min. A description of the radar and observational procedures is given by Eccles (1975).

2. General features

a. *Character of the environment*

Circulation at the 500 mb level over northeast Colorado on the afternoon of 9 July 1973 was influenced by a large anticyclone centered over the plateau region of the western United States (Fig. 1). Diffluent northerly flow advected cooler air southward during the day and had a destabilizing effect favoring convective development, which began in the NHRE research area by mid-afternoon.

Surface analysis at 1500 MDT[3] showed low pressure in western Kansas with cyclonic and confluent northeasterly flow over northeastern Colorado. This zone of confluence is reflected in detail by analysis of wind observations from the NHRE mesoscale surface network (Fig. 2). Surface moisture was relatively abundant with the mixing ratio (r) ranging between 8 and 10 g kg^{-1} and showing a typical decrease from southeast to northwest across the network. Potential temperature (θ), on the other hand, increased from the southeast toward the northwest largely in response to upward sloping terrain and associated decreasing surface pressure. The opposing potential temperature and moisture gradients produced a field of equivalent potential temperature (θ_e) which, with the exception of two stations on the southern extremity of the network, could be regarded as nearly uniform.

Special serial soundings from five stations designated in Fig. 2 are used to identify the local static stability and representative vertical wind shear. Temperature and dew point curves (Fig. 3) measured during ascent of a 1630 release from STK are chosen as representative of the storm's environment, because of the sounding's optimum location relative to the storm. The pseudo-

[3] All subsequent references to time will denote Mountain Daylight Time (MDT).

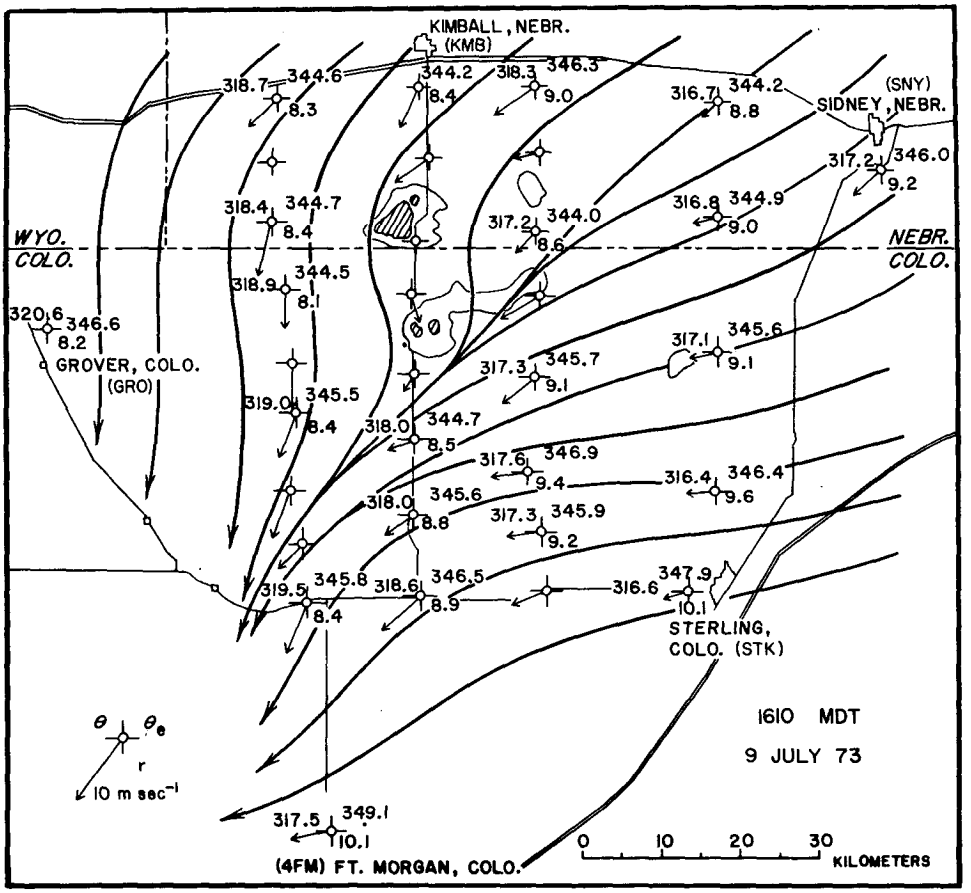

FIG. 2. Surface streamlines at 1610 MDT, 9 July 1973, over NHRE mesoscale network. Plotting model (lower left) includes wind (m s^{-1}), potential temperature (θ), equivalent potential temperature (θ_e), and mixing ratio (r). Special rawinsonde sites are located near Grover (GRO), Ft. Morgan (4FM), and Sterling (STK), Colorado, and at Kimball (KMB) and Sidney (SNY), Nebraska. PPI radar echo contours at 10 dB intervals above 30 dBZ show location of earliest thunderstorm developments.

adiabat having $\theta_e = 345.5$ K represents saturated conditions at cloud base measured there by a research aircraft, Queen Air (N10UW), operated by the University of Wyoming (Part II). Cloud base altitude was 3.8 km MSL[4] and θ, r, and static pressure were 316.5 K, 9.5 g kg^{-1}, and 650 mb, respectively. A lifted parcel with these properties would experience a temperature deficit up to 610 mb and 4 to 5°C temperature excess in the layer between 550 and 250 mb. We note that cloud base θ is 2 to 3 K colder then the environment; a common observation in updrafts beneath High Plains thunderstorms (Marwitz, 1972a; Foote and Fankhauser, 1973).

The inset in Fig. 3 gives the profile of θ_e with respect to pressure from the STK 1630 and GRO 1735 soundings. Values near the surface are consistent with conditions shown in Fig. 2. Both curves indicate a decrease to near 500 mb that is characteristic of a summertime convectively unstable atmosphere in northeast Colorado. The coldest and driest air aloft is found on the upwind GRO sounding where a layer from 550 to 475 mb has values $\leqslant 330$ K, with a minimum near 327 K.

Wind distribution in the vertical from three soundings is plotted in Fig. 3. The lowest level designates surface wind and all others are means for layers of 50 mb thickness. Conditions on the STK 1630 soundings are most representative of the environment in the layer from the surface to cloud base, while those on the GRO 1735 and KMB 1725 ascents best depict the environment in the cloud-bearing layer. We see that subcloud winds backed from east-northeasterly near the surface to light northerly near cloud base. Backing continued in the cloud-bearing layer from northerly to westerly near cloud top. Radar echo tops were recorded as high as 14 km. Wind shear in the layer from cloud base to cloud top (650–150 mb) was computed from the average of the three wind soundings to be 2×10^{-3} s^{-1}. According to the classification by Marwitz (1972b), a low to

[4] Unless otherwise specified all subsequent altitudes will refer to height above mean sea level (MSL). Height of the ground in the area of the storm was ~1.4 km.

moderate shear such as this is typical of environmental conditions surrounding multicell storms. Subsequent radar analyses will show that storm features on this day were indeed characterized by periodically evolving multicellular echo patterns.

b. Radar echo history

In the early afternoon small short-lived cells emerged from convective clouds forming near the foothills of the Rocky Mountains to the west and southwest of the NHRE area. By 1530 radar echoes appeared about 50 km northeast of the Grover site in convection developing over the Plains. A complex of multicellular thunderstorms moved southward from the position of PPI echoes shown in Fig. 2 and passed over the western portions of the NHRE precipitation and mesonetworks while under the surveillance of the diverse observational facilities. A major span of this system's lifetime, which extended from 1603 to 1821 (2.3 h), is represented by the low-level PPI scans shown at 15 min intervals in Fig. 4. At about 1830 a new echo cluster appeared in western Nebraska and was tracked as it proceeded southwestward across the sensor network. Finally a third development following essentially the same path as its predecessor moved from the vicinity of Sidney, Neb., and eventually dissipated within the NHRE area around 2230. In conjunction with these three major systems an enormous number of "initial" radar echoes developed both within and adjacent to their primary areas of influence. Of these, ~80% were shortlived and did not mature to become major cells.

Although firm statistics are not yet available, the multicellular developments on this day seem to be typical of the most frequent type of thunderstorm occurring in northeast Colorado. Less typical were the observed storm movements. In contrast to the normal case where the surface wind has a component opposite to the general storm motion individual storms moved virtually parallel to and faster than the local surface wind vector. The position of early echo developments is shown in Fig. 2 to be just north of a surface confluence zone. Echoes forming to the north of the confluent asymptote moved with a predominately northerly component while those forming to the south moved from

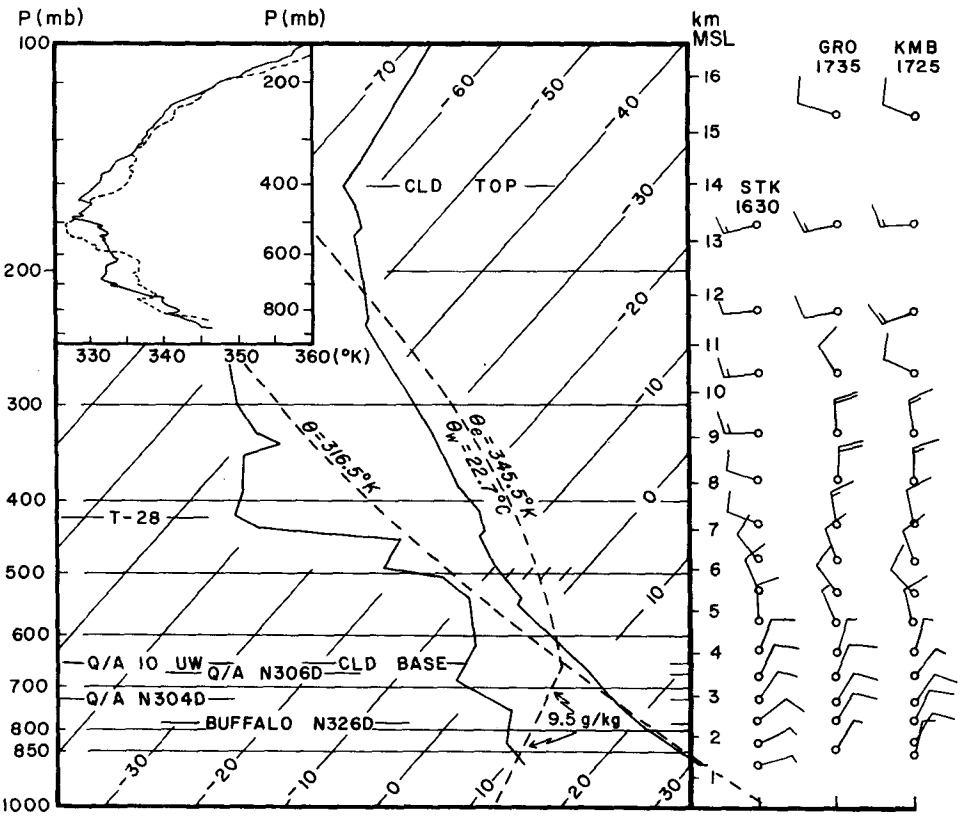

FIG. 3. Thermodynamic diagram showing temperature (T) and dew point (T_d) from STK 1630 sounding. Labeled dashed curves designate dry and moist adiabats and mixing ratio representative of measured cloud base conditions. Constant pressure levels sounded by instrumented aircraft (Part II) are designated at lower left. Surface wind and 50 mb layer-averaged winds (m s^{-1}) from three representative soundings are on the right. A full barb is 10 m s^{-1}.

Inset shows $\theta_e(K)$ vs pressure (mb) for STK 1630 (solid) and GRO 1735 (dashed) soundings.

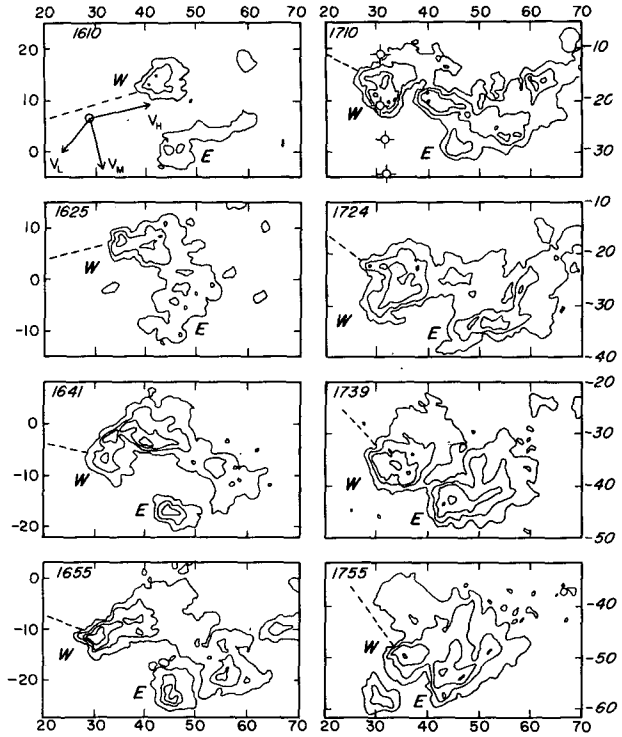

FIG. 4. Low level (1.4° EL; ~3 km MSL) computer-generated PPI radar reflectivity contours (at 10 dB intervals above 30 dBZ) at approximately 15 min intervals showing translation and evolution of multicellular thunderstorm systems on 9 July 1973. Two primary echoes comprising the overall system are identified as storm W and storm E on each scan. Labeling on border indicates distance in kilometers east and south of NHRE research radar located at Grover, Colo. Dashed lines on each frame point to the radar's location. Wind vectors on 1610 panel show simplified hodograph of environment winds with vectors representing mean winds in the subcloud, $\mathbf{V}_L$, cloud bearing, $\mathbf{V}_M$, and cloud top, $\mathbf{V}_H$, layers (10 m s^{-1}=10 km). Stars on 1710 panel designate locations of surface mesonetwork sites where meteorological variables and precipitation from storm W were measured.

the northeast. This behavior essentially reflects the surface wind flow.

Analyses to follow will focus on the individual storm, located on the western edge of the earliest echo complex, identified in Fig. 4 by the letter W. Cellular patterns at the times chosen to demonstrate echo configurations and translation do not reveal any obvious evidence of discrete propagation. Subsequent detailed analyses will however, reveal this to be a primary feature of the storm's behavior pattern.

c. *Precipitation*

Hailpads[5] and weighing raingages at four locations, designated on the 1710 panel in Fig. 4, recorded hailstone size and total precipitation during the direct overhead passage of the intense core of storm W. Average rainfall accumulation at the four sites amounted to 12 mm and the peak rainfall rate was near 120 mm h^{-1}. Of the many thunderstorms of the day, storm W was the only one to pass over hailpads located at the four sites. Thus, although hailpad data are not time-resolved, recorded events could be attributed uniquely to storm W. Analysis of these pads showed that hailstone size ranged from 0.3 cm to 1.6 cm, diameter, with a median size of 0.5 cm. Although no hailstones were collected beneath storm W, ground chase crews did retrieve specimens which fell from storm E. Laboratory analysis (Knight *et al.*, 1974) of these revealed that about 75% grew from graupel embryos and 25% had centers comprised primarily of frozen drops. A rough comparison of raingage and hailpad data indicates that less than 5% of the total mass of precipitation from storm W fell as hail.

From aircraft wind and moisture measurements, Fankhauser (1974) found that the rate of water vapor inflow to storm W was ~2.5 kt s^{-1}. The corresponding rate of water deposition measured at the ground was ~1.0 kt s^{-1}, leading to a precipitation efficiency of about 40%. Both the inflow and output were nearly an order of magnitude less than that found by Foote and Fankhauser (1973) for a hailstorm of the supercell type which formed in a highly sheared environment, but precipitation efficiency was somewhat greater in the present case. This result is in line with the inverse relationship between shear and precipitation efficiency proposed by Marwitz (1972c).

3. Formation and evolution of the cells

a. *The evolving three-dimensional structure*

As shown in Fig. 4, both storm W and storm E were at most times composed of numerous cells which on first inspection appeared to grow and decay in an apparent random manner. Close examination of cells comprising storm W, however, revealed that they evolved with a systematic behavior. The three-dimensional structure of this storm is shown as a function of time in Fig. 5 by PPI tilt sequences. Stepped altitude scans presented at ~15 min intervals are chosen to emphasize five discrete echo entities (identified by boxed labels) first appearing in the altitude range of 5.6 to 9.1 km (MSL) at locations to the south and ahead of the main echo. Cells are labeled according to their sequential order of appearance (e.g., W1, W2 ... Wn) and continuity for the four earliest developments is traced by dashed lines sloping downward with time. For example, cell W1 appearing on the 7.2 and 9.1 km scans at 1616 represents the first discrete development and is seen on later sequences (1631 and 1647) to descend and move through the echo complex as cells W2 and W3 form and progress in like manner. Nearly vertical dashed lines are included to show vertical continuity of mature cells at the time of each new echo formation. Cross

[5] Basic characteristics and measurement capability of the hailpad used in NHRE are described by Nicholas (1975).

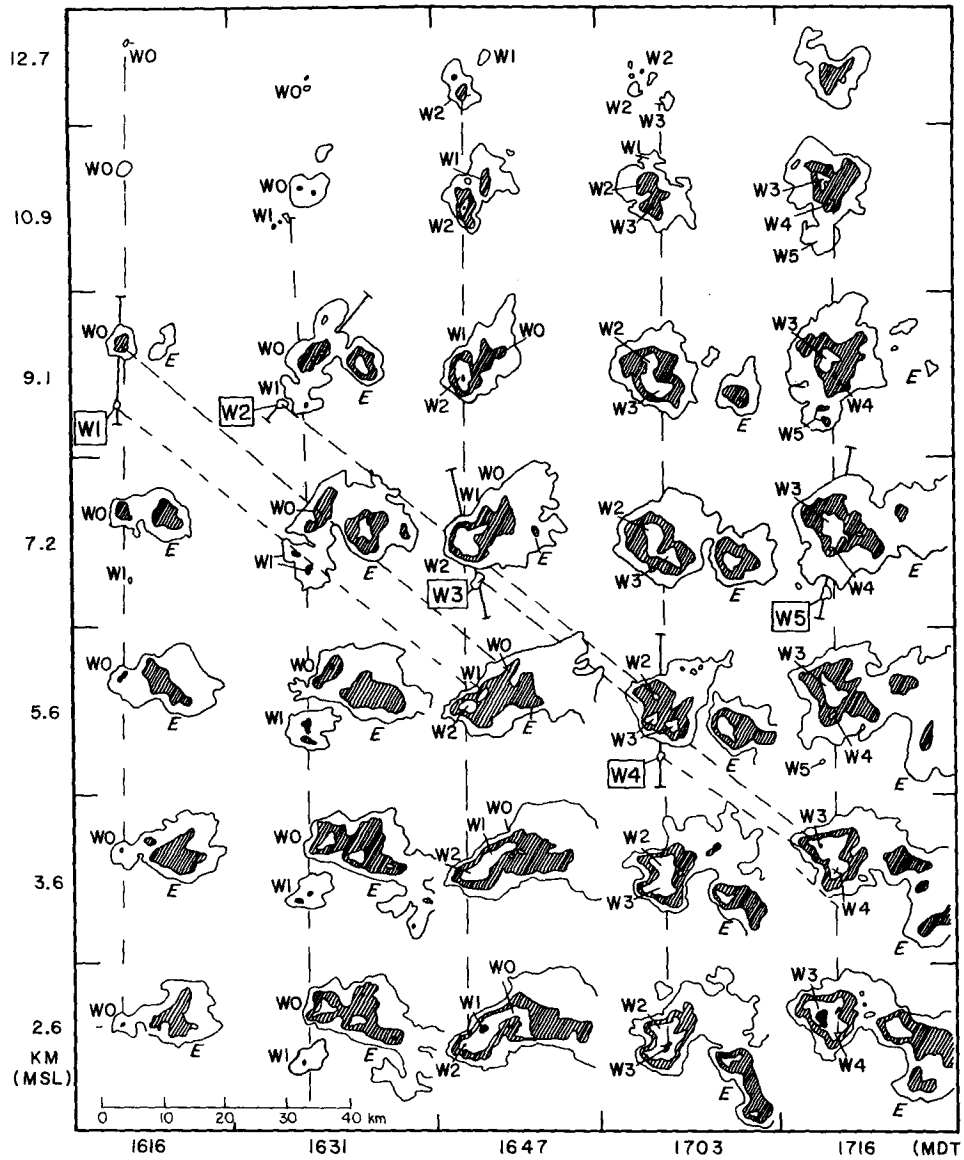

FIG. 5. PPI scans at elevations centered at altitudes indicated on the left. Radar reflectivity contours represent 10 dB intervals above 30 dBZ. Individual tilt sequences were obtained in a period of 120 s centered about the time labeled at the bottom of each. Discrete new cell formations W1 through W5 are identified in boxes. Downward sloping dashed lines give examples of vertical and temporal continuity of cells W1 through W4. Vertical dashed lines show vertical continuity of mature cell at each time. Individual cells are identified at all altitudes and times where continuity was established. Line segments show orientation of vertical sections in Fig. 6.

sections of radar reflectivity in Fig. 6 show the two-dimensional radar structure in vertical planes aligned along line segments shown at selected altitudes on the PPI scans in Fig. 5.

Common features of cells W1 through W5, evident in Figs. 5 and 6, are an average altitude of first appearance near 7 km and a tendency to form at a distance of 5 to 10 km ahead of the southward-moving complex at intervals of about 15 min. They all grow rapidly in size and intensity, moving in a relative sense toward the main echo, soon becoming its primary component. As shown at 1631, 1703, and 1716 MDT in Fig. 6, as many as three in the series of five cells coexist in varying stages of development. For instance, when W5 first appeared shortly before 1716, W4 was approaching maturity and W3 was in the early part of its decaying stage. Whereas the multicell model of Marwitz (1972b) specifies lateral alignment of coexisting cells across the direction of overall storm motion, Figs. 5 and 6 show that the cells in this case tend to be aligned along the direction of system movement.

The structure on the right of the vertical reflectivity

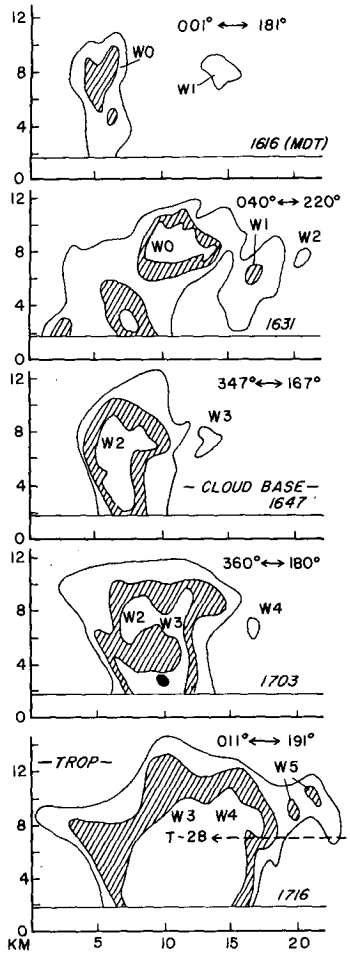

FIG. 6. Vertical cross sections of radar reflectivity aligned along line segments shown for each time in Fig. 5. Reflectivity contours represent 10 dB steps above 30 dBZ. Cells are labeled as in Fig. 5. Horizontal and vertical distance scales are equivalent. The height of the tropopause and the altitude of an aircraft penetration (Part IV) are indicated on the 1716 cross section.

profiles in Fig. 6, particularly at times 1631, 1703, and 1716 MDT, is rather similar to the weak echo region (WER) associated with updraft regions in supercell phenomena (Browning, 1964; Marwitz, 1972a; and Chisholm, 1973). Marwitz (1972b) and Chisholm and Renick (1972) point out that weak echo regions are also common features of multicell storms but that they are transitory and occur as a result of the discrete echo recurrence in the forward sector of the storm. In contrast to the persistent overhang in the supercell case, we conclude that the echo overhang depicted at times 1631 and 1716 in Fig. 6 is formed by new echo developing adjacent to and quickly joining existing mature and decaying cells. In both the supercell and multicell cases, however, the overhang implies the existence of updrafts supporting suspended precipitation particles.

The cells identified in Figs. 5 and 6 were not the only cells appearing in the storm between 1610 and 1730 MDT; there were many smaller ones which grew and decayed rapidly, having only a minor effect on the storm's overall configuration and evolution. There were also a few stronger cells which appeared periodically in a WSW direction and close to (within 3 km) existing mature W cells, about 15 min after their appearance as a first echo. The evolution of these was not easily distinguishable from that of the W cells but they are thought to be peripheral developments related to updraft circulations supporting the primary W cells. Since the W cells labeled 1 through 5 seemed to have the dominating influence on the storm's propagation, we will give special attention to their formation and evolution.

b. Location of new cells

The actual horizontal location of each new cell formation is shown in Fig. 7 with time and approximate

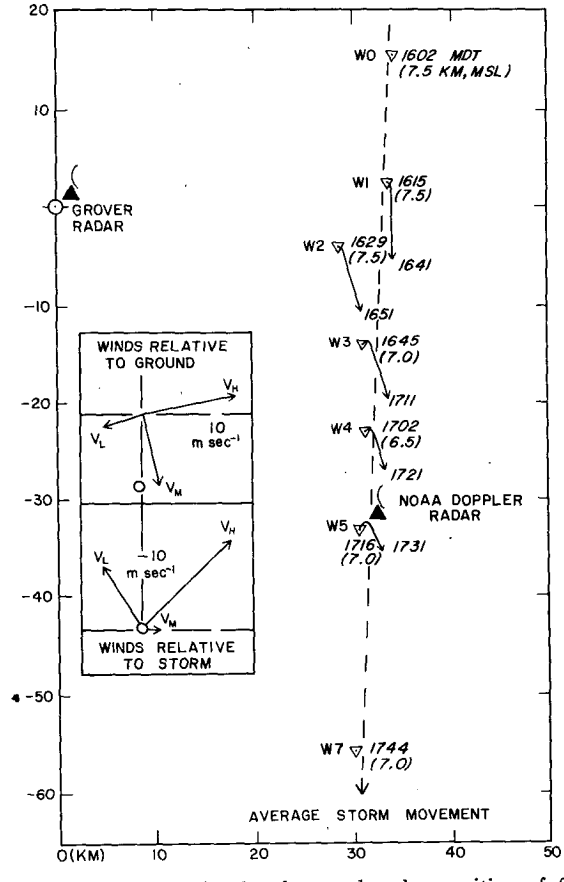

FIG. 7. Inverted triangles denote the plan position of first echo appearance for cells W0 through W7. Time and altitude (parenthesis) of first appearance are also indicated. Arrows show the paths of cells W1 through W5 from first detection to maximum reflectivity. The time when each was lost as an entity is plotted at the end of the respective tracks. Locations of the Grover radar and a NOAA Doppler radar (Part III) are indicated.

Inset gives environmental winds relative to the ground and to the storm (designated by a circle) for three layers; subcloud, V_L, middle troposphere, V_M and upper troposphere, V_H.

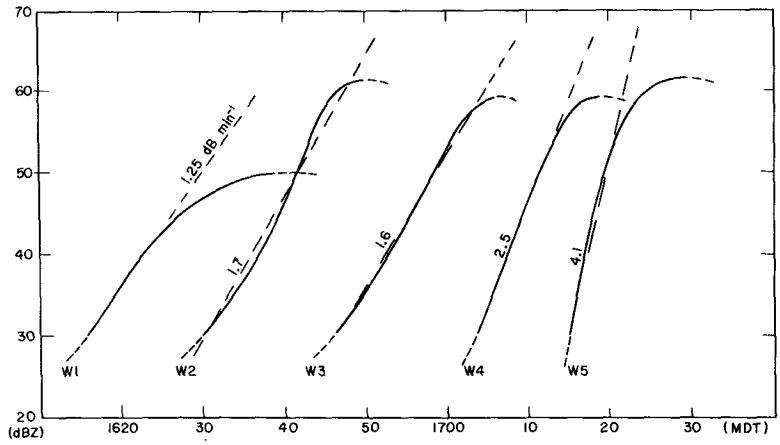

FIG. 8. Curves showing the growth of radar reflectivity (dBZ), for each cell as a function of time. Dashed lines show slopes used to obtain intensification rates indicative of the early history of each cell.

height of first echo detection also indicated. The locus of points identifying new cell appearance forms nearly a straight line which represents the direction of motion for the storm as a whole. As mentioned in Section 2 this was essentially parallel to the direction of surface winds along a zone of surface streamline confluence.

New cells appear at intervals of 13 to 16 min, and at locations approximately 10 km south of the formation point of the preceding developments. This sequence is broken between 1716 and 1744, as an anticipated development corresponding to W6 did not occur. We note, however, that a cell identified as W7 appeared 28 min after W5 at a distance of 2×10.5 km south of the W5 formation point and since these time and space increments are twice the period and separation of earlier developments we include it in the W series. The close proximity of new cell formation to the location of surface convergence maxima at the storm outflow-inflow interface (Part II) suggests that the periodicity in new cell development may have been related to the downdraft production by preceding cells during their intense and decaying stages.

c. *Tracks of individual cells*

Paths of cells W1 through W5 are shown in Fig. 7 for the length of time each was a distinguishable entity. For the most part, this period includes the time from first radar detection through intensification to maximum reflectivity. Following first appearance, each of the radar echoes grew rapidly in size, intensity, and vertical extent. During these early stages they were nearly stationary with respect to the ground and some even showed a tendency to move somewhat northward; a direction opposite the overall storm movement. During their later developing and mature stages, the paths of all cells are shown to follow about the same direction, moving from an azimuth of 340° to 350°, which is in agreement with the direction of $\mathbf{V}_M$, in Fig. 7 (upper, inset). Since no southerly flow was observed in the subcloud or middle tropospheric layers of the environment, the short period of stationarity or slight northward movement can be explained only by propagation of the radar echo through the updraft due to successive particle growth preferentially to the rear (north) of the updraft. After ascending beyond 7 km the echoes apparently accommodated to environmental steering winds and began their south-southeastward travel. During decay (not shown in Fig. 7) upper portions of the echo comprised of particles with low terminal fall velocities moved toward the northeast with a velocity of the high level relative winds ($\mathbf{V}_H$, in Fig. 7, lower inset), while lower and larger particles influenced the overall storm velocity during descent in strong downdrafts associated with the zones of maximum low-level reflectivity shown in Figs. 5 and 6 (see also Doppler radar observations discussed in Part III).

d. *Evolution of individual cells*

Intensification of cells W1 through W5 with respect to time is given by the growth curves of reflectivity factor Z (dBZ) in Fig. 8. The 15 min periodicity for new cell development is again demonstrated here. The average rate of echo intensification for the various cells increases with time from about 1 dB min^{-1} for cell W1 to $\sim$4 dB min^{-1} for W5. The fastest growth, that of W5, is about half the rate reported by Browning and Atlas (1965) for the early stages of a tornadic Oklahoma thunderstorm but about the same as the rate computed from data presented by Renick (1971) pertaining to a multicell hailstorm in Alberta. The indicated increase of growth rate with time may be related to a corresponding increase in the strength of updrafts supporting the later cells and/or to changes in the size and distribution of aerosols. Since subcloud thermodynamic characteristics along the path of the storm were fairly uniform in time and space (Part II), the increase was not likely

to be dominated by static stability variations and we look to increasing mesoscale convergence and to the possible ingestion of larger aerosols as explanatory mechanisms. Visible dust curtains rising at least halfway from the surface to cloud base were observed at the interface between inflowing and outflowing air by research aircraft during the latter stages of the storm's history. Surface convergence is discussed further in Part II but no direct measurements of aerosols were available in the present case.

The radar history of cell W5 is represented in Fig. 9 by the development of radar reflectivity contours as a function of height and time. According to Fig. 8, W5 was one of the most intense cells in the series. Detailed radar data showed that its maximum reflectivity reached 68 dBZ below cloud base at about 1733. Profiles similar to Fig. 9 constructed for the other cells showed that maximum echo tops for each cell increased progressively with time from about 12 km for W1 to ≥ 14 km for W5. The height of Z_{max} displayed a general tendency to increase accordingly. This supports the speculation that the strength of updrafts supporting successive cells also increased with time. All other characteristics of the evolution of the W cells were similar to those of W5 and we will center the discussion of their general behavior around the profile in Fig. 9.

The locus of circles plotted at 1 min intervals in Fig. 9 is intended to represent the history of precipitation particles influencing the evolution of cell W5. The ascent rate of visual turrets deduced from cloud photography taken between 1655 and 1715 was between 5 and 10 m s^{-1}. This was used to approximate the particle trajectory between 1700 and 1715 (the time of first echo for W5). From 1715 onward the path traces the history of the maximum reflectivity, assumed to be the trajectory of the largest particles. The rationale for relating the particle growth cycle to the history of the maximum reflectivity rests on the dominant dependence of radar reflectivity on particle size.

Of the 30 to 35 min total lifetime from air parcel entry at cloud base through first echo to the arrival of the Z_{max} at the ground, about 15 min is spent in rather slow ascent in the rising turrets comprising the shelf cloud to the south of the main system (see Fig. 1, Part II). The temperature scale on the left in Fig. 9 shows that undiluted air parcels undergoing moist adiabatic ascent would have a temperature of -12°C at the average level of first echo appearance (7 km). Subsequent to first detection the center of highest reflectivity ascended rapidly to an altitude of $\sim$9 km. At about the same time two closely spaced reflectivity maxima appeared. These are evident on the vertical

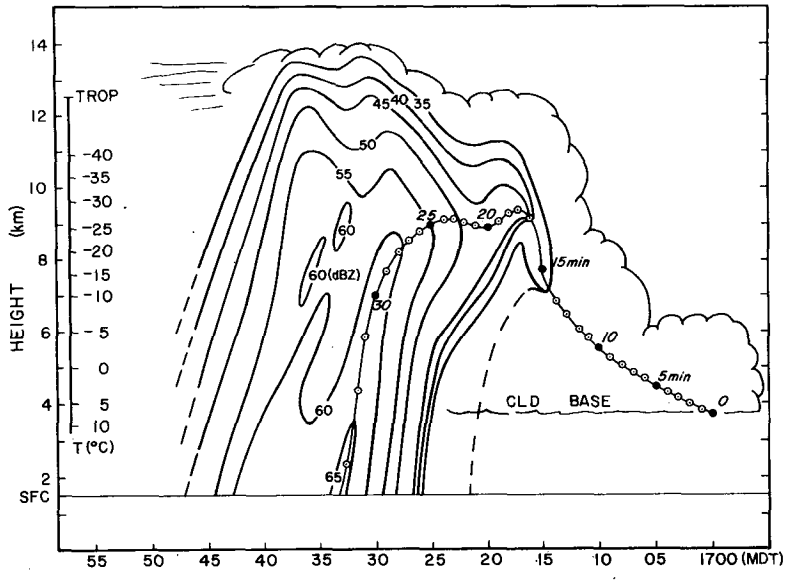

FIG. 9. Time-height profile of the radar reflectivity contours for cell W5 at 5 dB intervals above 35 dBZ. The echo profile as shown represents the history of particles that remained aloft for the longest period of time. The dashed 35 dBZ contour represents the history of echo which descended most rapidly after the first echo appearance. The locus of circles plotted at one-minute intervals represents the history of an air parcel which enters through cloud base, ascends in the turrets of the shelf cloud and grows particles large enough to produce the first echo at an altitude of $\sim$7 km. From that point onward in time the path follows the maximum reflectivity. Schematic cloud heights in the shelf cloud and at time of first echo are derived from time lapse photography and were used to estimate ascent rate prior to first echo.

The temperature scale on left represents moist adiabatic conditions for undiluted saturated ascent from cloud base.

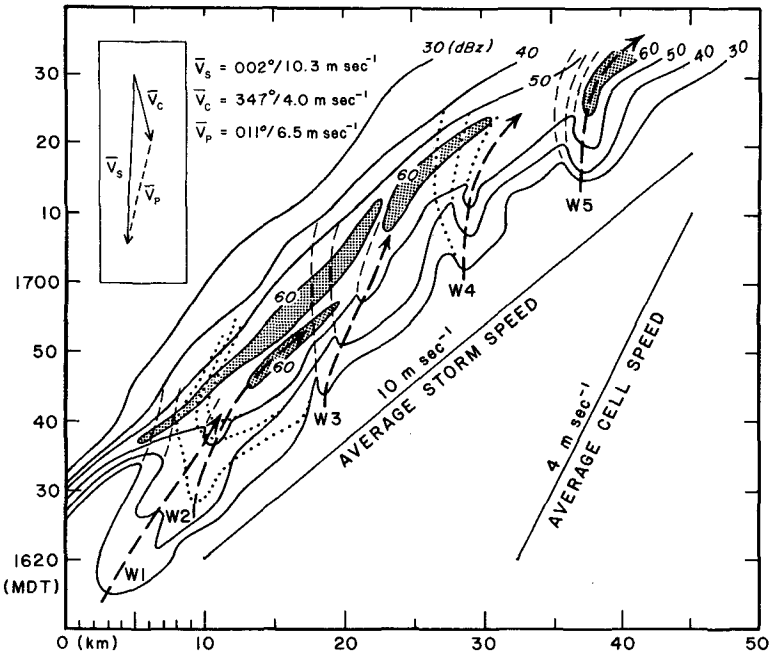

FIG. 10. The leading (rhs) and trailing (lhs) edges of reflectivity contours, usually in the altitude range of 4 to 8 km, for storm W as a whole (solid), and for the cells periodically forming to sustain it (alternating dashed and dotted), shown as a function of time. The abscissa denotes distance in kilometers essentially due south from a point near the origin of W1. Sloping lines give the speeds of the average storm and cell motions.

Vector diagram in the inset summarizes the relationship between cell, $\bar{\mathbf{V}}_c$, and storm, $\bar{\mathbf{V}}_s$, motion. The difference between the two represents the contribution to the storm's translation made by discrete propagation, $\bar{\mathbf{V}}_p$.

section at 1716 in Fig. 6. The profile in Fig. 9 represents the history of the reflectivity maximum nearer the forward edge of the storm. The one to the rear descended toward the surface at an earlier time and the history of its leading edge is represented by the dashed 35 dBZ contour. In addition to this double structure in Z_{max} along the vertical plane, analysis of cross sections adjacent to those used to construct Fig. 9, indicated that radar echo in the northeast sector of W5 also formed and descended earlier than did the contours as shown in Fig. 9. Both of these factors account for the lack of agreement between intensification rates shown for W5 in Figs. 8 and 9. The reflectivity contours in Fig. 9 trace the history of particles that remained aloft for the longest period of time and these had slower intensification rates than those used to produce the W5 curve in Fig. 8.

Following ascent to near 9 km the maximum reflectivity remained suspended there for a period of 10 to 12 min. During most of this time it resided in a region where the in-cloud temperature was less than −20°C. When radar reflectivity reached 55 dBZ, descent of Z_{max} toward the ground began; at first slowly but with a rapid cascade during the final 3 to 5 min. During these latter stages the slope of the high reflectivity contours with time gives a descent rate of about 30 to 35 m s^{-1}. Maximum observed downdraft was ~15 m s^{-1} (Part III), and the terminal fall velocity of the largest observed hailstones (1.5 cm, diameter) would be ~20 m s^{-1} so that there is reasonable agreement between the radar echo history, hailstone size, and measured Doppler downdraft velocity.

4. Storm motion in relation to the translation and propagation of individual cells

For examining the relationship between cell motion and the movement of the overall storm we refer to Fig. 10 which gives a continuous plot of radar reflectivity contours as a function of time along a y-axis which is aligned along the north to south direction of storm movement. At any instant the forward and trailing edges of storm W, usually in the altitude range of 4–8 km, are represented by the outer (30 dBZ) contours of the radar echo band. Interior contours similarly represent the leading and trailing edges of the higher reflectivity levels. For the most part, the leading edge (greatest y at any x and z at a given t) is defined by the leading edge of the newly forming W cells whose individual histories are traced by the heavy arrows. Alternating dashed and dotted contours, superimposed on the continuous contours show the history of the

trailing edges of the individual cells for the periods that they existed as discrete entities. Since they formed mainly to the south of the main system, their trailing edges consistently appeared at y-values greater than contours tracing the continuity of the overall storm. With time, however, the contours of individual cells show a tendency to blend toward equivalent contours along the trailing edge of the main swath as the cells lose their identity and become components of the main echo complex. Cell W2 which formed on the right flank of W1, and slightly to the north of the leading edge of existing echo (see PPI tilt sequence at 1631 in Fig. 5) was tracked along a different y-axis than that followed by the main system until it became a part of the overall complex. This explains why its leading edge appears at smaller y in its early stages.

Most of the cells, particularly W2, W4, and W5, exhibit a tendency to move more slowly in their early stages and to gradually tend toward the velocity of the storm as they intensify. The early period of slow movement very likely corresponds to the period of strongest updrafts and as updrafts decreased, partly in response to water loading associated with increasing reflectivity, the cells tended to assume the velocity of the mid-level ambient wind (see Fig. 7, inset).

Closed 60 dBZ contours (shaded streaks) of varying duration and length appear in Fig. 10 toward the end of each cell's traceable history. These vary in length from 6 to 20 km and in duration from 12 to 33 min. The one of longest duration seems to have been formed successively by two or more cells (W0, W1, and W2) so that an average length and duration would be somewhere between 6 and 10 km and 10 to 12 min, respectively. Ground areas below these high reflectivity streaks are reasonably the most favored regions of hailfall and very likely correspond to the hailstreak phenomena discussed by Changnon (1970). Although "ground truth" measurements were not available, hail was apparently generated and deposited at the ground in a cyclic manner related to the periodic evolution of individual updrafts through the multicellular storm.

Slopes of y with respect to time shown in Fig. 10 give the average speed for both the storm, $\mathbf{V}_s$, and its cell, $\mathbf{V}_c$. Directions of cell and storm movement are taken from Fig. 7. Vectors representing the average storm ($\bar{\mathbf{V}}_s$) and cell ($\bar{\mathbf{V}}_c$) velocities are plotted in the inset. Subtraction of the cell motion vector from the average overall storm motion gives the resultant labeled $\bar{\mathbf{V}}_p$. This vector has a magnitude of 6.5 m s^{-1} and represents the component of storm velocity contributed by discrete propagation through new cell development on the right forward flank of the storm. Reference to Fig. 5 shows that the orientation of $\bar{\mathbf{V}}_p$ represents the general direction for the location of new cell formation with respect to the existing echo. Since propagation contributes 6.5 m s^{-1} to the storm movement and discrete propagation occurs at a period of 15 min (900 s), we would expect the separation between existing radar reflectivity maxima and new echo to be around 6 km on the average. Figure 6 shows that at the time of first echo appearance the distance between new and mature elements varies from 5 to 10 km, in fair agreement with the anticipated value.

Thus, in summary, the motion of the main body of the storm was the result of two components; one due to the advection of individual cells along the direction of middle level winds and slightly to the left of the overall storm movement, and another due to the periodic and discrete propagation by new cell formation on the right forward flank of the echo. In the present case it is clearly the propagative component that has the dominant influence on overall storm motion. These results are similar to the general multicellular model proposed by Browning and Ludlam (1960), which has been found applicable in other High Plains thunderstorm studies by Marwitz (1972b) and by Chisholm and Renick (1972).

5. Summary

We have analyzed in considerable detail the radar structure of one of the many multicellular thunderstorms that occurred in northeast Colorado on 9 July 1973. The hailstorm receiving our concentrated attention had a lifetime of nearly 2 hours and was comprised of at least seven distinct cells which dominated its overall behavior. With maximum radar tops of 14 km and maximum hail size of 1.5 cm, diameter, the storm can be classified as moderate in intensity.

A periodic mode of cell development and evolution was characterized by discrete propagation of new cells forming at an average altitude of 7 km (−12°C) on the storm's right forward flank, 5 to 10 km ahead (south) of existing storm components at a frequency of about once every 15 min. This infrequent rate of new cell development may be compared to an average of one every 5 min found in an Alberta hailstorm similarly analyzed by Renick (1971).

After first radar detection all cells grew rapidly in size and intensity and, by moving more slowly in their early stages than the overall echo, soon became the main storm component. Average lifetime of individual cells, including the time from visually perceptible turrets to "first echo" through decay, was 45 min. Of this period, 30 to 35 min was radar-detectable history; approximately 15 min being spent in growth of precipitation particles to radar detectable sizes during ascent from cloud base (3.8 km) to the altitude of first detection by radar. With a formation interval of 15 min and a cell lifetime of 45 min, at any instant as many as three cells were found to coexist in varying stages of development. At a particular stage in the evolution of each cell, a vertical two-dimensional radar structure resembling the weak echo region and forward overhang typical of supercell thunderstorms was observed. In

contrast to the supercell case, these features were quite transitory and a result of the new echoes joining with the main echo soon after their formation as discrete entities.

Overall storm motion, from the north at an average speed of 10 m s^{-1}, was dominated by the propagation of the cells on its right forward flank. The average speed of cells was only 40% of the storm speed, hence the propagational component contributed well over half the storm's motion. Cell motion was quite slow in early stages of growth but tended with time toward the direction of the wind in the middle troposphere and eventually moved with about half its speed. After maturity and during decay the upper portions of the cells were carried out in the anvil in the northeastward direction of relative winds at the high levels (10–12 km), while the lower parts moved southward as components of the main body of the storm.

Although the general characteristics and behavior of individual cells were similar, as might be expected some irregularities and variations were observed. Maximum radar echo tops, maximum radar reflectivity, and intensification rate all showed a tendency to increase with time, and this increase appeared to be related to a corresponding increase in the strength of updrafts supporting the successive cells.

Consistent with the evolving radar structure, bands of high reflectivity appearing on *y-t* plots (Fig. 10) suggest that hail production at the ground occurred in streaks and this "bandedness" indicates that there was one major precipitation burst per cell. Largest hailstones measured at the ground were 1.5 cm in diameter. Analysis of time lapse photography of growing cloud turrets and the subsequent history of maximum reflectivity as it evolved from first echo through descent to the ground indicates that the total time available for growing hailstones of the observed size within the individual cells was between 30 and 35 min. Of this period, dwell time at temperatures lower than −20°C was on the order of 10 to 12 min.

Thermodynamic variables and airflow structure near and beneath storm W are elaborated in Part II of this series. Parts III and IV present internal airflow and microphysical measurements and Part V summarizes and synthesizes the complete observational set.

REFERENCES

Browning, K. A., 1964: Airflow and precipitation trajectories within severe local storms which travel to the right of the winds. *J. Atmos. Sci.*, **21**, 634–639.

——, and F. H. Ludlam, 1960: Radar analysis of a hailstorm. Tech. Note No. 5, Dept. of Meteor., Imperial College, London, 106 pp.

——, and D. Atlas, 1965: Initiation of precipitation in vigorous convective clouds. *J. Atmos. Sci.*, **22**, 678–683.

Changnon, S. A., Jr., 1970: Hailstreaks. *J. Atmos. Sci.*, **27**, 109–125.

Chisholm, A. J., 1973: Alberta hailstorms, Part I: Radar studies and airflow models. *Meteor. Monogr.*, **14**, *No. 36* Boston, Amer. Meteor. Soc., 1–36.

——, and J. H. Renick, 1972: The kinematics of multicell and supercell Alberta hailstorms. Alberta Hail Studies 1972, Research Council of Alberta, Hail Studies Report No. 72-2, 24-31.

Eccles, P. J., 1975: Developments in radar meteorology in the National Hail Research Experiment to 1973. *Atmospheric Technology* Fall-Winter 1974-75, National Center for Atmospheric Research, Boulder, Colo., 34-45.

Fankhauser, J. C., 1974: Subcloud air mass and moisture flux attending to northeast Colorado thunderstorm complex. *Preprints, Conf. Cloud Physics*, Oct. 1974, Amer. Meteor. Soc. Boston, 271–276.

Foote, G. B., and J. C. Fankhauser, 1973: Airflow and moisture budget beneath a northeast Colorado hailstorm. *J. Appl. Meteor.*, **12**, 1330–1353.

Knight, C. A., N. C. Knight, J. E. Dye and V. Toutenhoofd, 1974: The mechanism of precipitation formation in northeastern Colorado cumulus. I. Observations of the precipitation itself. *J. Atmos. Sci.*, **31**, 2142–2147.

Marwitz, J. D., 1972a: The structure and motion of severe hailstorms. Part I: Supercell storms. *J. Appl. Meteor.*, **11**, 166–179.

——, 1972b: The structure and motion of severe hailstorms. Part II: Multicell storms. *J. Appl. Meteor.*, **11**, 180–188.

——, 1972c: Precipitation efficiency of thunderstorms on the High Plains. *Preprints, Third Conf. Wea. Modification*, Rapid City, S. D., Amer. Meteor. Soc., 245–247.

Nicholas, T. R., 1975: Surface hail instrumentation in the NHRE. *Preprints, NHRE Symposium/Workshop on Hail and Its Suppression*, Estes Park, Colo. (unpublished manuscript).

Renick, J. H., 1971: Radar reflectivity profiles of individual cells in a persistent multicellular Alberta hailstorm. *Preprints, Seventh Conf. Severe Local Storms*, Amer. Meteor. Soc. Boston, 63–70.